Wear 502-503 (2022) 204378

Contents lists available at ScienceDirect

Wear

journal homepage: www.elsevier.com/locate/wear

Experimental investigation of erosion due to nanofluids

Marthe Braut [a], Luis González-Fernández [b], Anna Kosinska [c,*], Yaroslav Grosu [b,d], Pawel Kosinski [a], Boris V. Balakin [c]

[a] University of Bergen, Department of Physics and Technology, Postboks 7803, 5020 Bergen, Norway
[b] Centre for Cooperative Research on Alternative Energies (CIC energiGUNE), Basque Research and Technology Alliance (BRTA), Alava Technology Park, Albert Einstein 48, 01510 Vitoria-Gasteiz, Spain
[c] Western Norway University of Applied Sciences, Department of Mechanical and Marine Engineering, Bergen, Inndalsveien 28, Norway
[d] Institute of Chemistry, University of Silesia in Katowice, Szkolna 9, 40-006 Katowice, Poland

ARTICLE INFO

Keywords:
Multiphase flows
Erosion
Nanofluids
Nanoparticles

ABSTRACT

The demand for efficient and sustainable energy is continuously increasing. Among the many technologies with great potential within this field are nanofluids. Nevertheless, there is still a considerable lack of information regarding their erosive effects on systems materials. In this research, the tribological behaviour of aqueous 1.33 wt% TiO_2 nanofluid was investigated when jet-impinged with an average velocity of 0.8 m/s at flat targets of various materials (plastic, copper, rubber). The target surfaces were analysed using scanning electron microscopy (SEM), energy dispersive x-ray spectroscopy (EDX) and X-ray diffraction (XRD). It was found that impinging TiO_2 nanofluid caused erosion of 282 g/(yr.mm^2) for copper and 212 g/(yr.mm^2) for plastic. In addition, a deposition of nanoparticles was found for rubber at rate of 2.7 kg/(yr.mm^2).

1. Introduction

Nanofluids are nanometer-sized particles dispersed in a base fluid such as water or oil. The added particles alter the chemical and physical properties of the base fluid, and perhaps the most interesting is the enhancement of the heat capacity and thermal conductivity [1]. This causes a significant improvement in terms of efficiency and economy when applied to energy systems.

Despite the very interesting advantages of the possible application of nanofluids, there are major drawbacks of solid particles dispersed in operating fluids. Although nanoparticles are of significantly small size, they have the potential to cause wear of surrounding material. In some applications, such as thermal solar energy, this can be partially avoided by replacing nanofluids with "black fluids", see e.g., [2–4]. For many other applications, however, there is a need to identify the tribological behaviour of nanofluids before using them in large industrial applications. Additionally, the performance of nanofluids is strongly connected to their stability, and the agglomeration of nanoparticles is a common problem in the manufacturing and application of nanofluids.

George et al. [5] studied the erosive effects of a 0.1%-volume TiO_2/water nanofluid on cast iron and aluminium. They conducted experimental tests at different velocities and impingement angles of 0°–90° (the impact angle was measured from a horizontal axis). Erosion was found at a maximum to be close to 90° for cast iron, and 20° for aluminium. The material removal of cast iron was mainly due to corrosion-assisted erosion, while the aluminium smoothening was identified as a result of mild abrasive erosion. Some degree of work hardening was also observed for both materials.

Recent studies [6,7] have investigated the effect of aqueous nanofluids, namely TiO_2, Al_2O_3, ZrO_2 and SiC impinging onto flat metallic targets of aluminium, stainless steel and copper. Stainless steel targets encountered negligible thickness reductions. Copper targets, on the other hand, eroded, and aluminium turned out to be the most sensitive material with significant mass losses. Also, metals' resistance to erosion has previously been shown to be proportional to their hardness [8,9]. Aluminium has a lower hardness than copper and is more chemically reactive than copper, which explains the larger mass loss. The nanoparticles shown to cause the largest wear were of the following materials: TiO_2, Al_2O_3 and ZrO_2.

Jet-impingement tests have found alumina/water nanofluids to erode both aluminium [6,10,11] and copper surfaces [6,10,12], but cause negligible erosive effects on stainless steel [6]. Additional tests found the flow of alumina/seawater nanofluids to result in mass loss of carbon steel due to the combined effect of erosion and corrosion [13,14].

A study by Rashidi et al. [13] isolated the effect of erosion alone and found erosive rates of alumina nanofluids (average particle of 20 nm) to increase by a factor of ~10% compared to its base fluid.

* Corresponding author.
E-mail address: anna.dorota.kosinska@hvl.no (A. Kosinska).

https://doi.org/10.1016/j.wear.2022.204378
Received 21 January 2022; Received in revised form 7 April 2022; Accepted 6 May 2022
Available online 13 May 2022

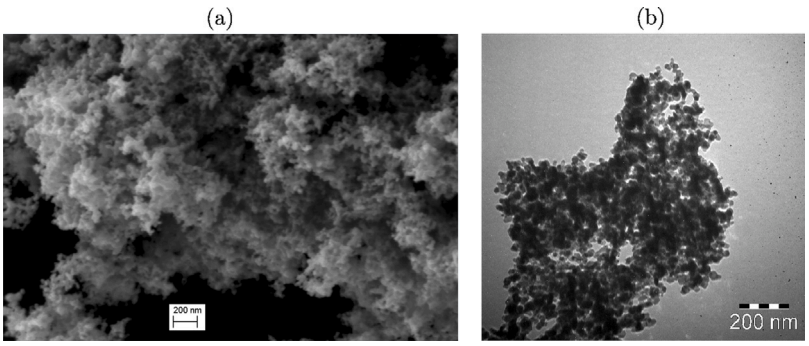

Fig. 1. (a) SEM (Jeol JSM-7400F, magnification 100k) and (b) TEM (Jeol JEM-1230, magnification 225k) images of dry TiO_2 nanoparticles.

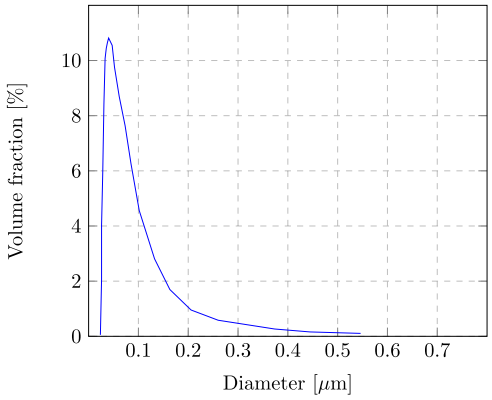

Fig. 2. Particle size distribution in the concentrated nanofluid.

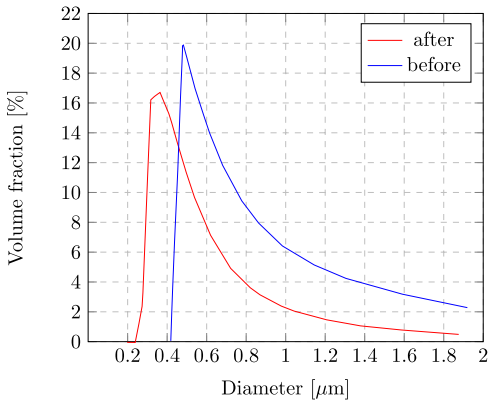

Fig. 3. Particle size distributions in the nanofluid before and after the experiment.

Another interesting finding is that by Bubbico et al. [6], namely that two different concentrations of Al_2O_3 in water were shown to erode aluminium at very similar rates.

Routbort et al. [15] performed tests of nanofluid erosion in a car radiator using SiC nanoparticles in water and CuO nanoparticles in ethylene glycol. No erosion was found for impact angles ranging from 30° to 90° on a Al3003 material surface. The only wear found in one case (CuO/water nanofluids) was corrosion, causing a material loss. In the following study, Routbort et al. [16] investigated the possible erosion of an impeller made of Al3003. CuO and SiC in ethylene glycol were used. No erosion was found after more than 700 h of impingement.

Jiang et al. [17] investigated the interaction of RAFM, 316L(N), and CuCrZr alloy with alumina–water nanofluids. The CuCrZr alloy

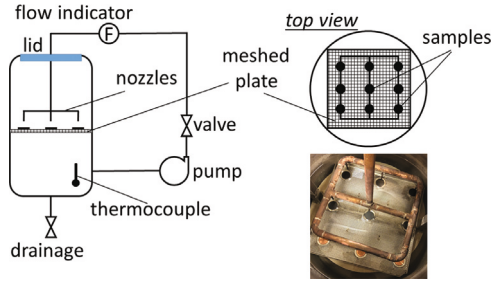

Fig. 4. Schematic description of the experiment and the photo of the tank with samples. There were 9 samples used to assure the repeatability.

Table 1
Properties of TiO_2 nanoparticles used in the research.

Property	Value
Density	4260 kg/m^3
Primary particle size	21 nm
Vickers hardness	1121 kg/mm^2 [6]
Molar mass	79.87 g/mol

revealed severe wear compared to the two other materials. The experimental results indicate wear as a function of test duration, fluid velocity, and particle concentration.

There exist few numerical studies with nanometer-sized particles in multiphase flows, despite significant amounts of similar studies with milli- or macrometer-sized particles. A numerical study conducted by Kosinska et al. [18] investigated the erosive effects of micro- and nano-sized particles in pipe elbows. As expected, increasing fluid velocity and particle diameter promoted the erosion rate. However, for particles smaller than 100 μm the maximum erosion rates reached the highest levels for smaller particles. This was explained by the formation of secondary flows pulling the smaller particles towards the elbow wall. Nevertheless, this did not occur to nanoparticles, as their low mass does not cause enough damage to erode the wall.

Safaei et al. [19] studied copper–water nanofluid numerically in 90° elbows. The results show maximum erosion rate, average erosion rate, and total erosion rate to increase with particle diameter, volume fraction, and fluid velocity. Erosion in pipe bends by micro- and nanoparticles (10^{-6} m and 10^{-9} m particle diameter) were also numerically investigated by Shinde et al. [20]. The erosion rate was found to be determined by particle impact angle and turbulence secondary flow. The micro-particles showed higher erosion compared to nanoparticles for nearly every operational condition. However, at bend angles higher than 100° and an identical radius of curvate, the erosion was nearly identical for micro- and nanoparticles.

Further experimental work is necessary to understand the erosion caused by nanofluids. To this date, the existing work covers different methods of identifying erosion. To be specific, most studies analyse the

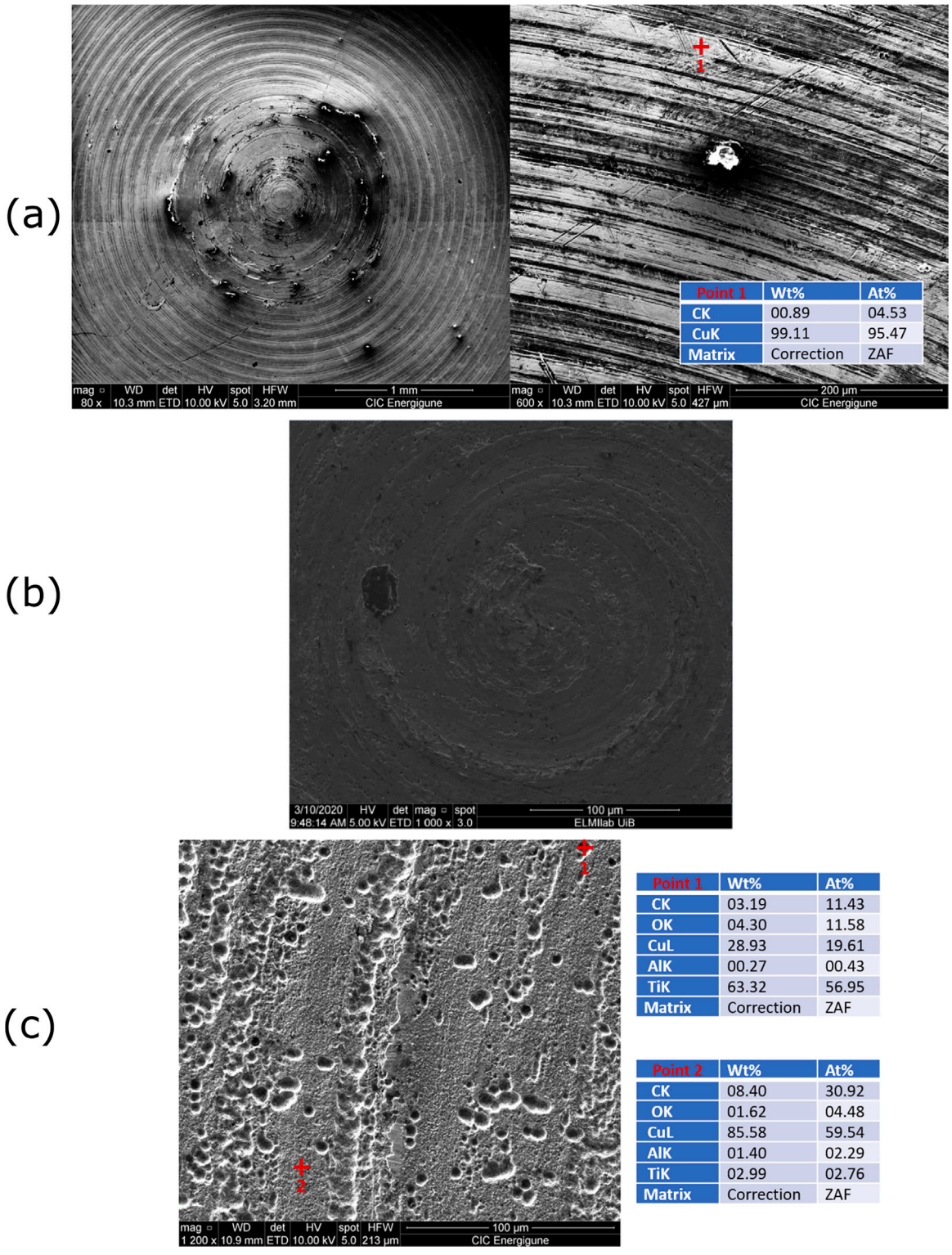

Fig. 5. Analysis of a copper sample for three cases: (a) SEM image of the initial surface at two different magnifications with compositional analysis; (b) SEM image of the surface after the first water test; (c) SEM image the surface after the final erosion test with compositional analysis.

target material by using profilometers and electron microscopy images. This provides information about the erosion pattern and magnitude. Few studies aim to find the quantitative wear, e.g., the mass loss and hence attain an erosion rate. Additionally, most present studies involve short-term erosion, but the possible applications of nanofluids require knowledge about long-term erosive effects. Therefore, we focused on these issues.

2. Experiment

In our research, we used titanium dioxide powder, with >99.5% purity (from Sigma-Aldrich). The nanofluids were produced by dispersing the nanoparticles in distilled water with surfactant. The surfactant was polyvinylpyrrolidone (PVP), also purchased from Sigma-Aldrich. Its mass fraction was the same as of the nanoparticles.

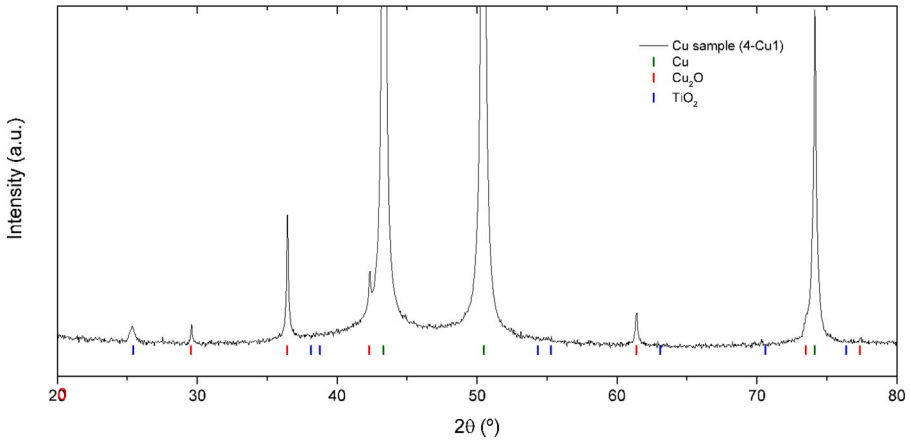

Fig. 6. XRD analysis of the treated copper sample.

Table 2
Mass change of the samples after two erosion tests calculated in units [g/year]. For some samples, we observe an increase of mass (depicted by plus).

		Water [g/yr.]	NF [g/yr.]	NF aver. [g/(yr.mm^2)]
Rubber	#1	+1.936	+2.020	2725
	#2	+1.850	+1.848	
	#3	+1.914	+1.494	
Plastic	#1	+ 0.182	−0.115	−212
	#2	+0.189	−0.128	
	#3	+0.181	−0.190	
Copper	#1	−0.0516	−0.175	−282
	#2	−0.0793	−0.190	
	#3	−0.0629	−0.193	

Fig. 1 shows microscopic images of dry TiO_2 nanoparticles. The figure shows that the particles in dry conditions form micro-sized agglomerates of primary particles. According to the datasheet from Sigma-Aldrich, the mean size of the primary particle was 21 nm. Other properties of the nanoparticles are depicted in Table 1.

The preparation of the TiO_2 nanofluid was done by using a two-step method. First, TiO_2, PVP, and distilled water were weighed separately by the use of a weighing scale (Kern 440-33N, with a precision of 0.01 g). Next, nanoparticles were dispersed in the distilled water, continued by the addition of the aforementioned surfactant. These components were then pre-mixed before being properly dispersed using an ultrasonic bath (Branson 3510) at 320 W for two hours. Finally, the finished nanofluid was visually examined for full dispersion. The fluids used in the experiments were analysed to find their particle size distribution using static light scattering (SLS) (Malvern Mastersizer 2000).

The test batch of the nanofluid was prepared in several stages. Initially, 1.0 litre of the nanofluid was produced in the sonicator at a mass concentration of 6 wt%. The particle size distribution in the concentrated nanofluid is presented in Fig. 2. The figure reveals that the mean particle size was about 50 nm. Also, the agglomeration of primary particles did not play an important role in the sample and the nanofluid was very stable.

Furthermore, to accumulate the desired volume of the nanofluid, five 1-litre volumes were mixed and matured for several days. The resulting particle size distribution shifted to the interval 400–1000 nm, and thus the stability of the nanofluid reduced, as seen in Fig. 3 (denoted as "before the experiment"). The last step of the nanofluid preparation was a dilution of 5 l of the nanofluid down to 1.3 wt% using tap water. The tap water was chosen as the main base fluid to maintain the physicochemical composition of the system. The rig was flashed with the tap water multiple times before operation and during trial runs. According to the SLS-analysis, the dilution procedure did not alter the particle size distribution.

Afterwards, a wet slurry erosion test was conducted in an experimental setup that is shown in Fig. 4. The rig consisted of a massive 30-l aluminium tank, a centrifugal pump (VLR 8 from Nocchi), a flow indicator (QN 1.5 from Werner Schutz), a K-type thermocouple, and a system of valves. The tank was equipped with a meshed plate, where nine samples of different materials were mounted in circular sample-holders. The role of the holders was to prevent the samples from sliding over the mesh. To avoid a reduction in fluid volume due to evaporation, a lid was mounted over the tank. The evaporated base fluid was condensed at the lid and recycled back into the system due to gravity.

Nine nozzles were located at a distance of 8 mm above the samples so that each of the nine samples was subjected to a vertical fluid flow impingement from the nozzles. The inner diameter of the nozzles was 3 mm, and they were connected to the mainline with an inner diameter of 16.2 mm. The length of the nozzles was 55.2 mm, and the distance between them was 120 mm. This distance was chosen to avoid any mutual influence of the jets from the neighbour nozzles. A supplementary computational fluid dynamics simulation of the rig confirmed that the nozzles could be considered as isolated [21].

We used three groups of samples of a different material. The materials chosen for this work were copper, plastic (PVC), and rubber (natural rubber). The copper and plastic samples were purchased from Astrup AS and the rubber sample from E Lund Maskin AS.

Each sample was cut into circular plates of 2 mm thickness and 29 mm diameter. Most experimental work done in the literature has investigated metals such as aluminium, stainless steel and copper. In our research, copper was selected as it is often used in heat transfer systems, but also as the resulting erosion rate can be compared to the rates found in the previous works. Additionally, rubber and PVC were chosen as they are softer materials so that one might expect a larger erosion rate compared to copper. Moreover, rubber and various plastic types are found in smaller components of heat transfer systems, which makes our study relevant for practical applications.

At first, tap water was added to the tank containing the target specimens. The system was left running for approximately a month at the flow rate of 0.19 m^3/h. An average flow velocity in a single nozzle was 0.8 m/s, which corresponded to the Reynolds number of 2400 (calculated using the nozzle diameter). The tap water test was done to investigate possible erosive effects due to contaminates coming into water from the environment and the elements of the rig. After shutting down the system, the target specimens were dried and weighted using an analytical balance (Sartorius CPA 324S) with a precision of 0.1 mg. After the background tap-water tests, the samples were cleaned with distilled water and flash-dried by compressed air from a laboratory pneumatic system.

(a)

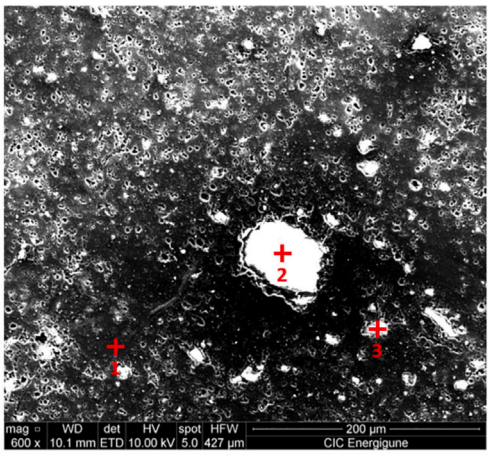

Point 1	Wt%	At%
CK	87.65	94.15
OK	02.41	01.94
NaK	00.57	00.32
AlK	00.06	00.03
SiK	00.17	00.08
SK	06.67	02.68
CaK	02.48	00.80
Matrix	Correction	ZAF

Point 2	Wt%	At%
CK	11.35	19.45
OK	29.62	38.11
NaK	00.70	00.63
MgK	00.52	00.44
AlK	20.43	15.58
SiK	29.49	21.61
SK	00.27	00.17
KK	07.09	03.73
CaK	00.53	00.27
Matrix	Correction	ZAF

Point 3	Wt%	At%
CK	11.90	19.97
OK	26.40	33.25
NaK	14.30	12.53
MgK	06.10	05.06
AlK	12.32	09.20
SiK	24.85	17.83
SK	00.53	00.33
KK	02.04	01.05
CaK	01.55	00.78
Matrix	Correction	ZAF

(b)

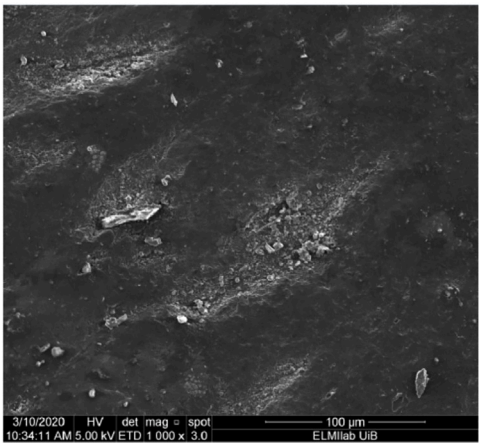

(c)

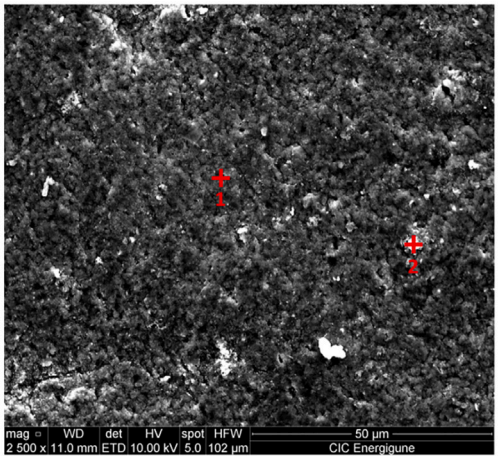

Point 1	Wt%	At%
CK	77.01	88.86
OK	03.70	03.20
NaK	00.24	00.14
MgK	00.10	00.06
AlK	01.72	00.88
SiK	01.03	00.51
SK	02.02	00.87
ClK	13.18	05.15
CaK	00.46	00.16
TiK	00.55	00.16
Matrix	Correction	ZAF

Point 2	Wt%	At%
CK	32.73	58.08
OK	09.68	12.89
NaK	00.95	00.88
MgK	00.29	00.26
AlK	00.59	00.47
SiK	00.52	00.39
SK	01.53	01.02
ClK	14.05	08.45
PdL	00.60	00.12
CaK	00.77	00.41
TiK	38.29	17.04
Matrix	Correction	ZAF

Fig. 7. Analysis of a rubber sample for three cases: (a) SEM image of the initial surface at two different magnifications with compositional analysis; (b) SEM image of the surface after the first water test; (c) SEM image the surface after the final erosion test with compositional analysis.

In the next test, 1.3 wt% nanofluid was circulated with the same flow in the system for 334 h. The particle size distribution shifted to the left as the heaviest particles were deposited in the rig. This is also depicted in Fig. 3. In addition, the agglomeration of the nanoparticles was probably hindered by the breakage of formed agglomerates in the pump and frequent collisions between the particles. It is important to note that, during the experiments, the temperature of the fluid increased by about 40 °C above ambient. This was caused by the work of the pump and the frictional losses in the fluid. After the test, the material samples were rinsed in distilled water, dried and weighed. Post-test images were taken by the use of scanning electron microscope (SEM), energy-dispersive X-ray spectroscopy (EDX) imaging and X-ray diffraction (XRD) analysis.

3. Results of the experimental analysis

3.1. The mass of target materials

The first source of erosion data was based on the mass loss of the material targets. The samples were weighed before and after both water tests and the erosion test. Furthermore, the data were treated to find the mass loss per unit time. The results can be found in Table 2.

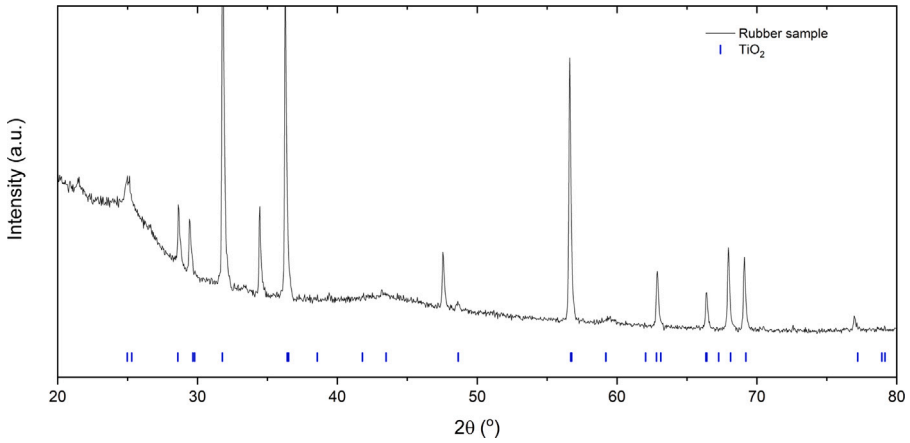

Fig. 8. XRD analysis of the treated rubber sample.

To begin with, the rubber targets encountered a mass increase from the erosion test, and with similar rates for both operational fluids. The most probable explanation is the penetration of particles from the fluid into the target. It is interesting to note that the mass increase is similar for both water and nanofluid test. It may indicate that the captured particles mainly originate from the eroding of the whole rig (the pump and pipes). This was confirmed by a supplementary SLS-measurement of the medium that revealed trace amounts of 20 μm particles.

When running the nanofluid test, the volume flow rate increased by 20% after 150 h from the start of the experiments. We connect this observation to a partial destabilization of the nanofluid when the agglomerated nanoparticles settled to the bottom of the tank. A respective reduction of the apparent viscosity of the dispersion resulted in a lower pressure loss in the system and the increase of the flow rate according to the pump curve. According to our estimation, the resulting concentration of nanoparticles was about 1.1 wt%. This value was obtained from the analysis of the pump curve, the corresponding pressure change due to the increased viscosity and the rheological expression by Roscoe and Brinkman [22].

The destabilization was confirmed by the SLS-analysis shown in Fig. 3 for a nanofluid sample taken after the experiment. The particle size distribution was shifted towards the lower sizes, which was due to the separation of larger particles from the pre-experimental distribution.

Considering the plastic targets, a mass increase was observed for each target after the water tests, while a mass loss was encountered after the nanofluid erosion test. Hence, the erosion by the solid nanoparticles seems to dominate the process and exceeds the large particle penetration into the target. We note the increase of the mass is significantly lower for the plastic targets in the tap-water test, if compared to the rubber targets. This is because the hardness of the plastic is about three orders higher than for the rubber. The mean mass loss rate for plastic targets is approximately a tenth of the observed rate by George et al. [5] who used aluminium and cast iron as target materials. Existing experimental research on the erosive effects of nanofluids have not studied target materials other than metals, reducing the ability to compare our results with the ones obtained by other researchers. Discussing the mechanisms of erosion in the nanofluid, we note that the Stokes numbers for the nanoparticles were of the order 10^{-6}-10^{-4}. Thus, in theory, light particles are not expected to collide frequently with the targets. However, the Brownian and the turbulent diffusion of the particles [23] towards the targets contribute to the erosion significantly when the number density of the particles is high. In addition, the lubrication forces (a repulsion acting on a particle as the fluid between the particle and wall is "squizzed") acting in the vicinity of the targets incline the nanoparticle trajectories and so sharpen the impact angles [24].

The copper targets encountered a mass loss for both tests. As seen in the table, there are differences between the erosion rates of water and the nanofluid as an operational fluid. The erosion rate caused by the TiO_2 nanofluid can be compared to the one reported by Nguyen et al. [11] for alumina nanofluids impinging onto an aluminium surface. They found a mass loss rate corresponding to 480 g/(yr.mm^2), which is around 70% more than in our work. Also, Celata et al. [7] investigated the erosive effects of TiO_2 onto a copper target. They found negligible erosion rates.

3.2. Wear track analysis by SEM, EDX and XRD

The surface of the samples was also analysed using SEM (Quanta 200 FEG) operated in a high vacuum mode. The images were acquired using the secondary electron detector with a relatively low accelerating voltage (10 kV) to avoid charging the samples, as two of the studied materials were non-conductive. In addition, compositional analyses were carried out by EDX.

The elemental analysis of the samples was performed by XRD (Bruker D8 Advance) equipped with a LINXEYE detector using CuKα radiation in θ–2θ configuration. The analysis was carried out at room temperature in the 2θ range from 20 to 80 degrees, with a step size of 0.04 degree and a counting time of 2 s per step. EVA software was used for the identification of the crystalline phases present in the diffractograms.

Fig. 5 shows images of the copper sample (taken at the different stages of the test). The image taken before the tests depicts circular structures obtained during machining of the samples, but the SEM–EDX analysis shows almost pure copper, as expected. The image taken after the first water sample shows a crater-like structure on the surface. This may have been due to macroscopic particles in the system, as already discussed. Therefore, the mass of the samples reduces during the experiments. The SEM–EDX analysis also reveals the presence of copper oxide (corrosion).

The elemental composition is shown in two different regions. As can be seen, the amount of titanium (indicating the presence of TiO_2) is significant all over the analysed surface, but it is much higher in the holes than in the flat regions. This suggests an accumulation of nanoparticles in the formed cavities.

To confirm the presence of TiO_2 by a complementary method, XRD analysis was carried out. The result for the copper sample is presented in Fig. 6 with the identification of the present phases. As can be seen, apart from Cu and Cu_2O, TiO_2 was also identified, which corresponds to the results of the SEM–EDX analysis. Additionally, the oxidation of the sample, corroborated by the presence of Cu_2O phase, can be assumed to be an effect of the test. This also shows that corrosion took also place.

The presence of corrosion in addition to erosion was also investigated by other researchers. For instance, Molina et al. [25] studied a

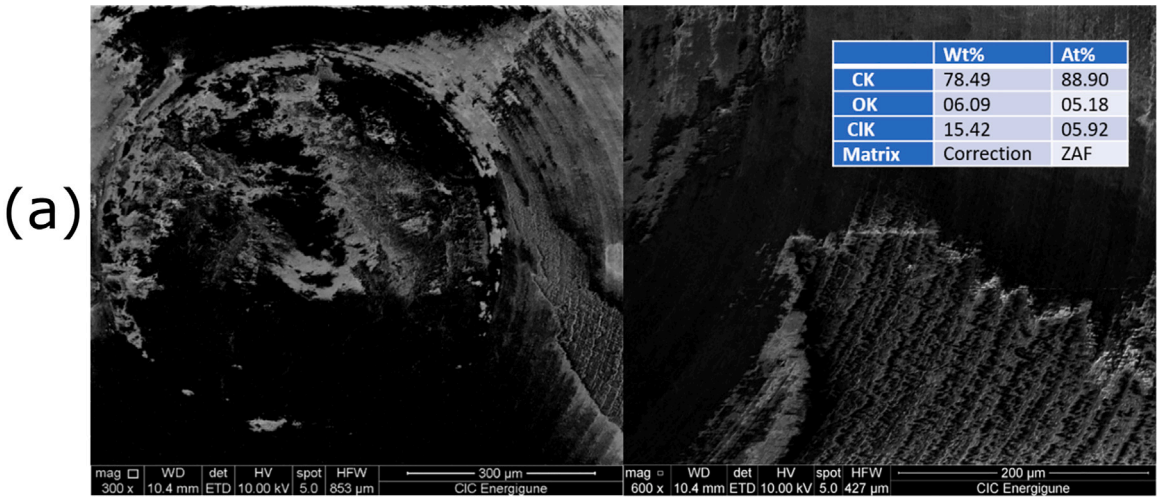

	Wt%	At%
CK	78.49	88.90
OK	06.09	05.18
ClK	15.42	05.92
Matrix	Correction	ZAF

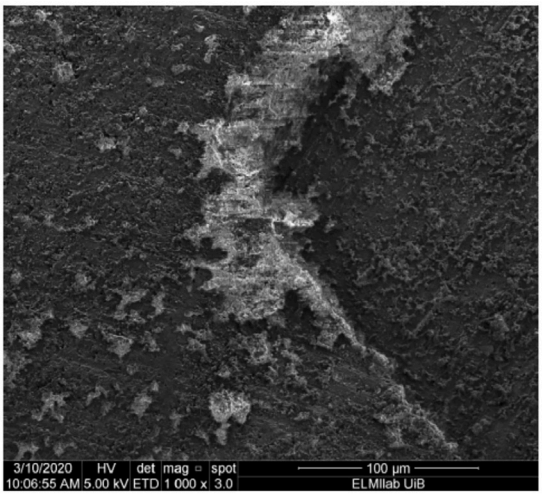

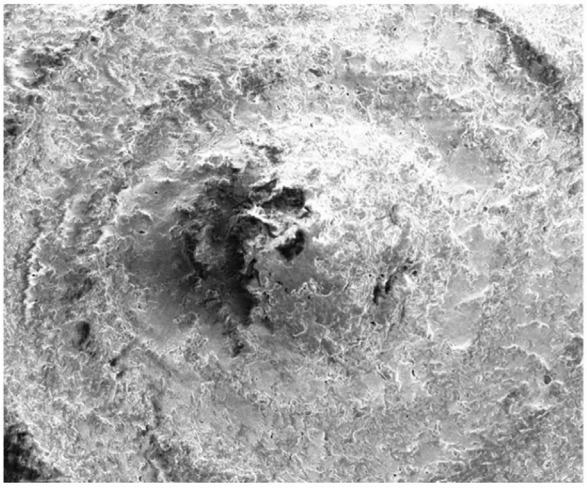

Element	Wt%	At%
CK	51.64	65.61
OK	25.90	24.70
AlK	02.67	01.51
SiK	00.79	00.43
ClK	15.17	06.53
TiK	03.82	01.22
Matrix	Correction	ZAF

Fig. 9. Analysis of a plastic sample for three cases: (a) SEM image of the initial surface at two different magnifications with compositional analysis; (b) SEM image of the surface after the first water test; (c) SEM image the surface after the final erosion test with compositional analysis.

system of alumina nanoparticles in water with ethylene-glycol. Also, in [26,27] alumina-nanopowders in water were used. Similarly to our research, they investigated the mass loss of specimens, supported by optical microscopy. Zhang et al. [28] investigated erosion and corrosion on aluminium alloy in ethylene glycol–water solution. They used an impingement-jet system, that is, our experimental set-up could also be compared to theirs. Finally, an analogous issue was addressed by [29], who studied CuO in water and ethylene glycol. However, all these papers involved combinations of different materials (types of particles and fluids) than those used in the present research.

The SEM results for one of the rubber samples are shown in Fig. 7. The surface of the initial sample is highly in-homogeneous, presenting a large number of holes and incrustations, with a different component balance. The first water test did not change the general surface structure, even though the total mass of the samples increased. This was most probably due to the deposition of the corroding elements of the

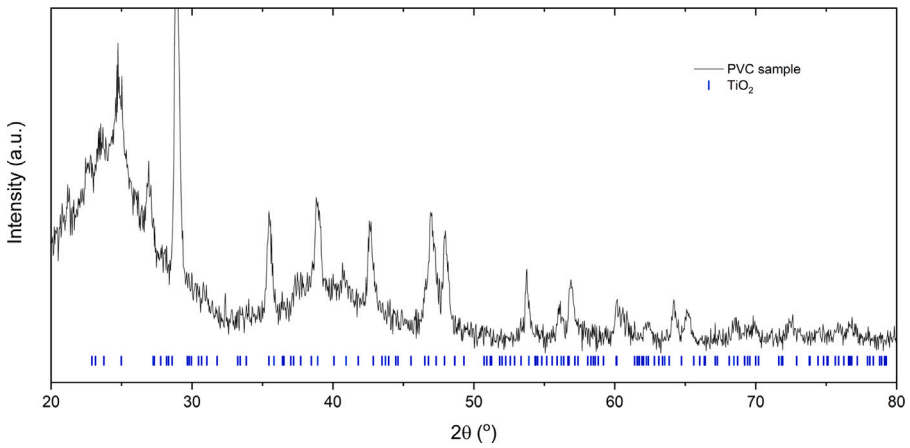

Fig. 10. XRD analysis of the treated PVC sample.

rig. Nevertheless, this possible phenomenon was not revealed in our SEM analysis. A possible explanation is that we spotted only some local deposition through the microscopy.

After the final erosion test, the deposition of TiO_2 on the sample surface also occurred. As for the copper sample, the distribution of TiO_2 is not homogeneous. Although it can be found in different regions, its amount is much more marked in the protuberances of white colour. The XRD analysis (Fig. 8) confirms the presence of the titanium oxide in the treated sample.

The investigation in the previous section revealed a mass increase in all the rubber samples. This occurred during both the water and nanofluid test. This would indicate that the rubber samples' erosion process was negligible compared to particles' deposition.

The analysis of one of the plastic samples is shown in Fig. 9. The surface gathered a significant amount of electric charge during the measurement, which made it challenging to perform the compositional analysis (the material is not conductive). Also, the surface was rough, which makes it more difficult to draw conclusions. Therefore, after the final erosion test, the presence of TiO_2 was determined by analysing the whole region of the image, i.e., not a punctual analysis as for the previous samples. The analysis reveals that particle deposition occurred. Reading the corresponding XRD report from Fig. 10, we confirm the uptake of titanium oxide by the PVC surface.

3.3. Roughness analysis

Raw and treated samples were also characterized by using a Bruker stylus profilometer DektakXT. The profile of each sample was determined for a 5 mm sampling distance on several regions of the samples.

Fig. 11 shows the surface roughness profiles of one of the copper samples. As seen from the figure, after the erosion test the surface of the sample presents a significantly larger roughness than the raw sample. Similarly, Fig. 12 shows profilometry curves for the plastic samples. However, the extent of the growth is lower for the plastic samples than for the copper samples: the erosion process results in a double-fold increase in the roughness due to the formed craters.

Finally, Fig. 13 shows roughness profiles of one of the rubber samples. The most remarkable effect of the erosion test is the appearance of the surface "deformation" in the order of micrometre-scale. In fact, this was also detected for the plastic samples, even though the effect was lower. A possible explanation is a low hardness of the sample material. Regarding the roughness itself, the effect is considerably lower compared to copper and PVC. This may confirm our previous analysis that revealed a limited effect of erosion on the rubber samples.

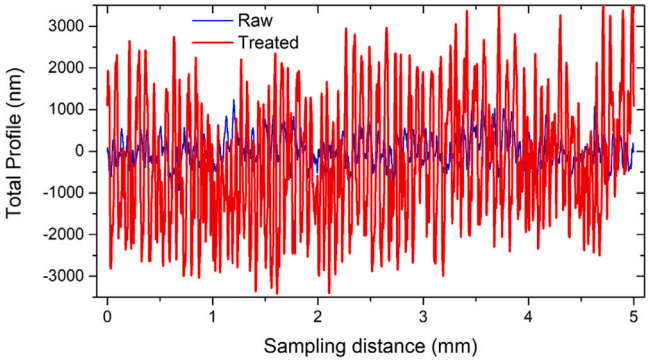

Fig. 11. Surface roughness profiles of raw and treated copper samples.

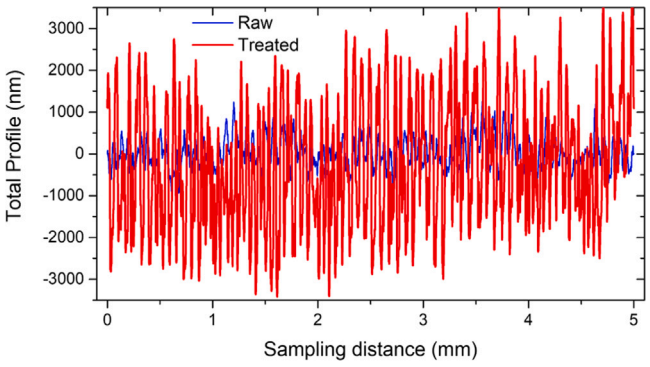

Fig. 12. Surface roughness profiles of raw and treated plastic samples.

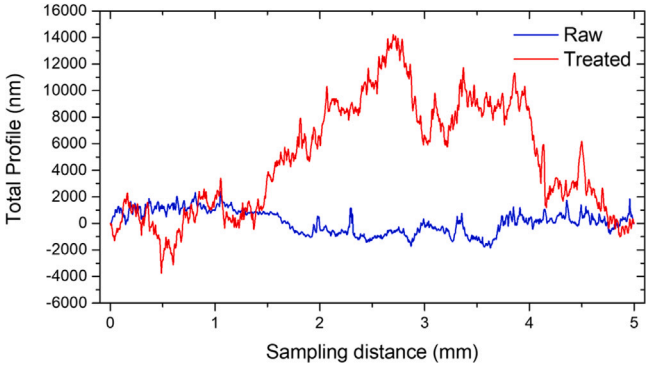

Fig. 13. Surface roughness profiles of raw and treated rubber samples.

4. Conclusions

In this research, an experimental method was applied to investigate the erosive effects of a solid–liquid flow onto a flat target. A set-up was developed to expose submerged targets to low-speed impinging TiO_2 nanofluids. The experiments revealed the erosion rates of 282 g/(yr·mm^2) and 212 g/(yr·mm^2) for copper and PVC respectively. The rubber samples increased their mass at 2.7 kg/(yr·mm^2).

In the process of nanofluid preparation, an increase in mean particle size was observed due to particle agglomeration. This issue occurred in the second stage of the process that was diluting the concentrated nanofluid with distilled water. This also shows that the erosion process may be more intense due to the presence of larger particles, even though the total number of particles is less so that the number of particle–wall collisions is reduced.

Another important challenge in this type of study is isolating the erosive effects. Nanoparticles tend to deposit on exposed surfaces and this influences the process. A possible mechanism is the formation of a protective nanoparticle layer. Also, an important issue is the formation of corrosion that may occur if one uses metallic surfaces in systems.

CRediT authorship contribution statement

Marthe Braut: Investigation, Writing – original draft. **Luis González-Fernández:** Investigation. **Anna Kosinska:** Conceptualization, Writing – review & editing, Supervision. **Yaroslav Grosu:** Investigation. **Pawel Kosinski:** Supervision, Conceptualization, Writing – review & editing. **Boris V. Balakin:** Supervision, Conceptualization, Methodology, Funding acquisition.

Declaration of competing interest

The authors declare that they have no known competing financial interests or personal relationships that could have appeared to influence the work reported in this paper.

Acknowledgments

We thank Harald Moen from the Western Norway University of Applied Sciences for his help with the construction of the experimental rig. The study was supported by the Research Council of Norway (project 300286).

References

[1] Y. Grosu, A. Anagnostopoulos, B. Balakin, J. Krupanek, M.E. Navarro, L. González-Fernández, Y.L. Ding, A. Faik, Nanofluids based on molten carbonate salts for high-temperature thermal energy storage: Thermophysical properties, stability, compatibility and life cycle analysis, Sol. Energy Mater. Sol. Cells 220 (2021) 110838.

[2] M. Alberghini, M. Morciano, L. Bergarnasco, M. Fasano, L. Lavagna, G. Humbert, E. Sani, M. Pavese, E. Chiavazzo, P. Asinari, Coffee-based colloids for direct solar absorption, Sci. Rep. 9 (2019) 4701.

[3] F.A. Essa, A.H. Elsheikh, A.A. Algazzar, R. Sathyamurthy, M.K.A. Ali, M.A. Elaziz, K.H. Salman, Eco-friendly coffee-based colloid for performace augmentation of solar stills, Process Saf. Environ. Prot. 136 (2020) 259–267.

[4] A. Kosinska, B. Balakin, P. Kosinski, Photothermal conversion of biodegradable fluids and carbon black nanofluids, Sci. Rep. 12 (3398) (2022) http://dx.doi.org/10.1038/s41598-022-07469-w.

[5] G. George, R. Sabareesh, S. Thomas, V. Sajith, T. Hanas, S. Das, C. Sobhan, Experimental investigation of material surface erosion caused by TiO2 nanofluid impingement, J. Nanofluids 3 (2) (2014) 97–107.

[6] R. Bubbico, G. Celata, F. D'Annibale, B. Mazzarotta, C. Menale, Experimental analysis of corrosion and erosion phenomena on metal surfaces by nanofluids, Chem. Eng. Res. Des. 104 (2015) 605–614.

[7] G. Celata, F. D'Annibale, A. Mariani, S. Sau, E. Serra, R. Bubbico, C. Menale, H. Poth, Experimental results of nanofluids flow effects on metal surfaces, Chem. Eng. Res. Des. 92 (9) (2014) 1616–1628.

[8] A. Reddy, G. Sundararajan, Erosion behaviour of ductile materials with a spherical non-friable erodent, Wear 111 (3) (1986) 313–323.

[9] G. Sundararajan, The solid particle erosion of metallic materials: the rationalization of the influence of material variables, Wear 186 (1995) 129–144.

[10] G. Molina, F. Aktaruzzaman, K. Martin, V. Soloiu, M. Rahman, Testing of wear and erosion effects of nanofluids on metals: New instruments and assessment methodologies, 2018.

[11] C. Nguyen, G. Laplante, M. Cury, G. Simon, Experimental investigation of impinging jet heat transfer and erosion effect using al2o3-water nanofluid, in: Proceedings of the 6th IASME/WSEAS International Conference on Fluid Mechanics and Aerodynamics (FMA'08), Citeseer, 2008.

[12] G. Molina, F. Aktaruzzaman, W. Stregles, V. Soloiu, M. Rahman, Jet-impingement effects of alumina-nanofluid on aluminum and copper, Adv. Tribol. 2014 (2014).

[13] A. Rashidi, M. Packnezhad, M. Moshrefi-Torbati, F. Walsh, Erosion–corrosion synergism in an alumina/sea water nanofluid, Microfluid. Nanofluid. 17 (1) (2014) 225–232.

[14] A. Rashidi, M. Paknezhad, M. Mohamadi-Ochmoushi, M. Moshrefi-Torbati, Comparison of erosion, corrosion and erosion–corrosion of carbon steel in fluid containing micro-and nanosize particles, Tribol.-Mater., Surf. Interfaces 7 (3) (2013) 114–121.

[15] J. Routbort, D. Singh, W. Yu, G. Chen, D. Cookson, R. Smith, T. Sofu, Effects of nanofluids on heavy vehicle cooling systems, in: Proceedings of the VT Annual Merit Review Meeting, Argonne National Laboratory, 2008, pp. 1–16.

[16] J. Routbort, D. Singh, E. Timofeeva, W. Yu, R. Smith, Erosion of radiator materials by nanofluids, Argonne Natl. Lab., Veh. Technol.–Annu. Rev. (2010).

[17] H. Jiang, W. Wang, D. Chu, W. Lu, D. Cheng, Y. Huang, Y. Wu, Corrosion-erosion tests of fusion reactor materials in flowing nanofluids, J. Nucl. Mater. 494 (2017) 361–367.

[18] A. Kosinska, B. Balakin, P. Kosinski, Theoretical analysis of erosion in elbows due to flows with nano-and micro-size particles, Powder Technol. 364 (2020) 484–493.

[19] M. Safaei, O. Mahian, F. Garoosi, K. Hooman, A. Karimipour, S. Kazi, S. Gharehkhani, Investigation of micro-and nanosized particle erosion in a 90 pipe bend using a two-phase discrete phase model, Sci. World J. 2014 (2014).

[20] S. Shinde, D. Kawadekar, P. Patil, V. Bhojwani, Analysis of micro and nano particle erosion by the numerical method at different pipe bends and radius of curvature, Int. J. Ambient Energy (2019) 1–8.

[21] M. Braut, Experimental and Numerical Investigation of the Erosive Effects of Micro-and Nanometer-Sized Particles in Water Flow (Master's thesis), The University of Bergen, 2020.

[22] W. Pabst, Fundamental considerations on suspension rheology, Ceramics Silik. 48 (1) (2004) 6–13.

[23] A. Guha, A unified Eulerian theory of turbulent deposition to smooth and rough surfaces, J. Aerosol Sci. 28 (8) (1997) 1517–1537.

[24] O.I. Vinogradova, G.E. Yakubov, Dynamic effects on force measurements. 2. Lubrication and the atomic force microscope, Langmuir 19 (4) (2003) 1227–1234.

[25] G.J. Molina, F. Aktaruzzaman, V. Soloiu, M. Rahman, Erosion-corrosion wear of heat-exchanger materials by water/ethylene-glycol/alumina nanofluids, Int. J. Surf. Eng. Interdiscip. Mater. Sci. 6 (2018) 1–22.

[26] G.J. Molina, F. Aktaruzzaman, V. Soloiu, M. Rahman, K. Martin, Development and assessment of a new flow-through test instrument to study wear and erosion effects of nanofluids, Int. J. Surf. Eng. Interdiscip. Mater. Sci. 5 (2017) 60–77.

[27] G.J. Molina, F. Aktaruzzaman, V. Soloiu, M. Rahman, K. Martin, Design and testing of a jet-impingement instrument to study surface-modification effects by nanofluids, Int. J. Surf. Eng. Interdiscip. Mater. Sci. 5 (2017) 43–61.

[28] G.J. Molina, F. Aktaruzzaman, V. Soloiu, M. Rahman, K. Martin, Investigation of erosion-corrosion of 3003 aluminum alloy in ethylene glycol-water solution by impingement jet system, Corros. Sci. 51 (2009) 283–290.

[29] S.Z. Heris, M. Shokrgozar, S. Poorpharhang, M. Shanbedi, N.S. H., Experimental study of heat transfer of a car radiator with CuO/ethylene glycol-water as a coolant, J. Dispers. Sci. Technol. 35 (2014) 677–684.